Interface Focus

rsfs.royalsocietypublishing.org

Review

Cite this article: Yasun E, Kang H, Erdal H, Cansiz S, Ocsoy I, Huang Y-F, Tan W. 2013 Cancer cell sensing and therapy using affinity tag-conjugated gold nanorods. Interface Focus 3: 20130006.
http://dx.doi.org/10.1098/rsfs.2013.0006

One contribution of 10 to a Theme Issue 'Molecular-, nano-and micro-devices for real-time *in vivo* sensing'.

Subject Areas:
biochemistry, nanotechnology, biotechnology

Keywords:
gold nanorods, surface plasmon resonance, photothermal therapy, aptamer, near infrared, photoacoustic imaging

Author for correspondence:
Weihong Tan
e-mail: tan@chem.ufl.edu

Cancer cell sensing and therapy using affinity tag-conjugated gold nanorods

Emir Yasun[1], Huaizhi Kang[1,2], Huseyin Erdal[1], Sena Cansiz[1], Ismail Ocsoy[1], Yu-Fen Huang[1] and Weihong Tan[1]

[1]Department of Chemistry and Department of Physiology and Functional Genomics, Shands Cancer Center and Center for Research at the Interface of Bio/nano, UF Genetics Institute and McKnight Brain Institute, University of Florida, Gainesville, FL 32611-7200, USA
[2]Department of Chemistry, College of Chemistry and Chemical Engineering, Xiamen University, Xiamen 361005, People's Republic of China

Through the developments in controlling the shape of gold nanoparticles, synthesis of gold nanorods (AuNRs) can be considered as a milestone discovery in the area of nanomaterial-based cancer treatments. Besides having tuneable absorption maxima at near infrared (NIR) range, AuNRs have superior absorption cross section at NIR frequencies compared with other gold nanoparticles. When this unique optical property is combined with the specificity against cancer cells used by affinity tag conjugations, AuNRs become one of the most important nanoparticles used in both cancer cell sensing and in therapy. In this review, the impact of size and shape control of nanoparticles, especially AuNRs, on cancer cell treatments and a range of aptamer-conjugated AuNR applications in this regard are reviewed.

1. Introduction

Gold nanoparticles (AuNPs) have been extensively used in biomedical applications owing to their biocompatibility, facile synthesis, easy surface functionalization and tuneable physical properties [1–3]. Their sizes and shapes can be varied for a particular biological application such as labelling, delivering, heating and sensing [2,4]. Sizes of AuNPs depend on the nature of the reducing agent that reduces the gold precursor and the molar ratio of the reducing agent or stabilizer to gold precursor used during synthesis [5,6]. Different shapes of AuNPs can generally be synthesized either using rigid templates such as porous alumina, polycarbonate membranes and carbon nanotubes or surfactants as soft templates [6–13]. Surfactants, which are also known as capping agents, interact with different growing faces of the nanoparticles to confine their shape, whereas rigid templates act as a mould to constrain the area of the metal precursor reduction [14]. For the shape control of nanoparticles, using surfactants eliminates the tedious steps of rigid template preparation and dissolving the rigid template contents to release the prepared nanoparticles at the very end. The change in the size and shape of AuNPs affects their absorption maxima that can vary in the visible–near infrared (NIR) range. The colour of the nanoparticles also changes depending on the absorption maxima variations. This tuneability of the optical absorption facilitates various biomedical applications including, but not limited to, colorimetric detection assays for proteins [15–18], DNAs [18–21] and cancer cells [22] that operate in the visible range; photothermal therapy [23–28], photoacoustic imaging (PAI) [29–34] and heat-induced drug delivery [35] that operate in the NIR range.

2. Tuning the surface plasmon resonance band of plasmonic nanoparticles to near infrared range

2.1. The importance of near infrared range in biological applications

Nanoparticles that have significant absorption in the tissue optical window (600–1300 nm), which is also known as NIR, are promising sensing and

Royal Society Publishing
Informing the science of the future

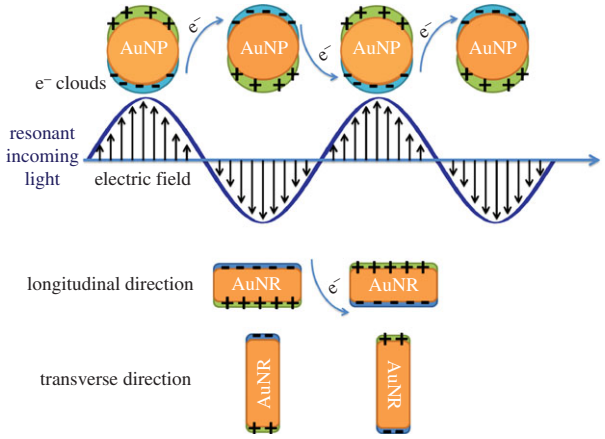

Figure 1. Surface plasmon oscillations in spherical gold nanoparticles (AuNPs) and gold nanorods (AuNRs).

therapeutical agents for cancer cell treatments, because healthy tissues do not absorb at this spectral region [36]. Moreover, in longer wavelengths the scattering of the light is minimized. Thus, the combination of the minimal scattering and NIR absorption allows deep tissue penetration [4,37,38]. This penetration depth can be 1–10 cm depending on the tissue types [38,39].

2.2. The impact of surface plasmon resonance band on nanoparticle-based cancer cell applications

When AuNPs absorb light, the oscillating electromagnetic field of the light triggers polarization of the conduction band electrons on the surface of the nanoparticles, and the polarized electrons go through collective coherent oscillations with respect to the positive ions in the metallic lattice; these oscillations are called as surface plasmon oscillations (figure 1). Because surface plasmon oscillation has the same frequency as the incident light, it is also known as surface plasmon resonance (SPR; [38]).

SPR frequency highly depends on the size and shape of the nanoparticles, as it was indicated before for the absorption maxima. For spherical AuNPs, there is only one SPR frequency, around 520 nm in the visible region, which is responsible for the intense red colour of the spherical AuNPs. For gold nanorods (AuNRs), there are two SPR frequencies, known as the longitudinal and transverse bands (figure 1). The transverse band is for electron oscillations that take place along the transverse direction (figure 1) and is a weak absorption band in the visible region similar to the SPR frequency of the spherical AuNPs. The longitudinal band is related to the electron oscillations along the longitudinal direction (figure 1) and is a strong absorption band in the vis-NIR region [38,40].

The excited surface plasmon electrons relax in two different ways: they can either emit the light that has the same energy as the incident light, known as SPR scattering, or they can transfer the absorbed energy to the metallic lattice in the form of thermal energy. Subsequently, the hot lattice cools down by phonon–phonon interactions and the heat is transferred to the surrounding medium [4,38,40]. This forms the basis of all plasmonic nanoparticle-based photothermal therapy applications. Because the SPR band of nanoparticles contains both scattering and absorption components, tuning the shapes and sizes of the nanoparticles can change their scattering and absorption properties dramatically [41]. For example, when the aspect ratio of the AuNRs increases, the longitudinal band undergoes a red shift and whereas the scattering component increases, the absorption component of the longitudinal band decreases [42]. Therefore, for NIR-imaging applications, larger AuNRs that have high scattering efficiency are preferred, and for photothermal applications, smaller AuNRs that have high absorption efficiency are preferred.

2.3. Comparison of the near infrared-absorbing gold nanoparticles

The most commonly used NIR-absorbing AuNPs for cancer cell sensing and therapies are gold nanoshells (AuNSs), AuNRs and gold nanocages (AuNCs). Because scattering and absorption properties of those AuNPs determine their efficiency in cancer cell treatments, these properties were compared by the discrete dipole approximation (DDA) method after adjusting their structures to tune their SPR bands to 800 nm. In order to have the SPR band at 800 nm, AuNRs should have an aspect ratio of 3.6 with a width length of 20 nm, AuNSs should have a gold shell thickness of 3.2 nm with a silica core diameter of 50 nm and AuNCs should have an inner edge length of 50 nm with a wall thickness of 6 nm. According to the DDA results, the absorption and scattering cross sections for AuNRs and AuNCs are comparable with each other and they are much larger than those for the AuNSs [37,41]. The extinction cross-section coefficients of the AuNRs and AuNCs are more than two times larger than that of AuNSs. This huge absorption cross section makes AuNRs and AuNCs good candidates as photothermal therapy agents [41]. For example, heating per gram of gold for AuNRs is at least six times faster than that for AuNSs [43].

Besides their easily tuneable structures for a particular cancer cell treatment, AuNRs should be further modified with affinity tags such as antibodies or aptamers to achieve specificity against cancer cells, while avoiding interference with healthy cells (table 1).

3. Synthesis, growth mechanism and surface modification of gold nanorods

3.1. Synthesis and growth mechanism

Besides the rigid template methods, AuNRs have been synthesized by many different surfactant-based methods such as photochemical [44], electrochemical [45] reduction methods and the seed-mediated [6,11–13,38] method. So far, the seed-mediated method is the most efficient method to synthesize AuNRs. In this method, there are two steps: the first step is the synthesis of the seed AuNPs and the second step is growth of these seeds into nanorods. First, single crystalline, seed AuNPs less than 4 nm are prepared by the reduction of auric acid ($HAuCl_4$) with ice cold sodium borohydride ($NaBH_4$) in an aqueous cetyl trimethylammonium bromide (CTAB) solution. Second, the growth solution is prepared by introducing ascorbic acid, as a mild reducing agent, into an aqueous CTAB solution of $HAuCl_4$ and silver nitrate ($AgNO_3$) to reduce Au^{3+} to Au^{+}. When the seed solution is added to the growth solution, seed AuNPs can catalyse the reduction of the Au^{+} to Au^{0} on their surface by the present

Table 1. Aptamer sequences with their corresponding target cells used in the illustrated studies.

aptamer name	sequences (5′ → 3′)	target cells	control cells	biomarker	K_d (nM)
KK1H08	ATC CAG AGT GAC GCA GCA GAT CAG TCT ATC TTC TCC TGA TGG GTT CCT AGT TAT AGG TGA AGC TGG ACA CGG TGG CTT AGT	K-562	CCRF-CEM, RAMOS	N/A	296 ± 41
Sgc8c	ATC TAA CTG CTG CGC CGC CGG GAA AAT ACT GTA CGG TTA GA	CCRF-CEM	RAMOS, NB-4	PTK7	0.78 ± 0.10
TD05	AAC ACC GGG AGG ATA GTT CGG TGG CTG TTC AGG GTC TCC TCC CGG TG	RAMOS	CCRF-CEM	IgM	74.7 ± 8.7

ascorbic acid. This leads to the addition of the gold atoms to the surface of the seed nanoparticles, resulting in the growth of nanorods. The role of the CTAB is that of shape templating surfactant. There are numerous hypotheses about the templating mechanism of CTAB in rod formation. In one of them, it is believed that CTAB is preferentially bound onto (110) or (100) faces of gold and it leaves the (111) face for the addition of gold atoms that results in the nanorod growth along the (100) face [46]. In the other mechanism, after ascorbic acid reduction of $HAuCl_4$ in the growth solution, $AuCl_2$ binds to CTAB to form the $AuCl_2$–CTAB complex. This complex binds to the tip of the seed AuNPs at a faster rate than to side faces, so that it leads to nanorod growth [47]. The addition of $AgNO_3$ to the CTAB solution results in the immediate formation of AgBr. It has been claimed that Ag^+ ions adsorb onto the surfaces of AuNPs in the form of AgBr, and Ag^+ is reduced to Ag atoms on the side (110) face of the nanorods at a faster rate than on the (111) end face. This avoids addition of gold to the side faces and thus results in nanorod growth. The aspect ratio of the AuNRs can easily be tuned by either varying the amount of seed solution or the amount of $AgNO_3$ added to the growth solution.

3.2. Surface modification of gold nanorods

Besides their unique optical properties, in order for AuNRs to show their efficacy in cancer cell treatments, their surfaces should be modified to further stabilize them in biological fluids and to allow targeted cancer treatments.

CTAB coating on the surface of AuNRs provides stability in their aqueous solutions, but it has been proved that in biological fluids, such as serum, CTAB-capped AuNRs can easily be precipitated. In order to avoid the precipitation and increase the circulation times of AuNRs *in vivo*, their surfaces are modified with polyethylene glycol (PEG; [43]) After PEG modification, AuNRs exhibited a circulation time of 17 h, and they maintained their longitudinal SPR band during this circulation time [43]. PEG-protected AuNRs can also decrease non-specific binding to the surfaces of AuNRs [48–50]. In order to PEGylate the surface of AuNRs, thiol (-SH)-modified PEGs are used to form covalent bonds between the sulfhydryl groups of PEG and the gold surface, which are also known as thiolate bonds.

Specificity against cancer cells can be achieved by tethering the affinity tags such as antibodies or aptamers on the AuNR surface for sensing and therapy applications. Antibodies can be adsorbed onto the AuNR surface by hydrophobic interactions with the polymer, polystyrene sulfonate (PSS) that had been previously adsorbed on the AuNR surfaces through electrostatic interactions [24]. Surfaces of the CTAB-capped AuNRs are positively charged, so the negatively charged PSS polymer can easily be adsorbed on the surface of AuNR via electrostatic interactions, followed by the adsorption of antibodies through the hydrophobic interactions with the PSS polymer.

As another affinity tag, aptamers are single-stranded oligonucleotides that bind to their specific target molecules, such as small bio-molecules and proteins, with affinities equal to those of antibodies. Aptamers have been generated by repeated rounds of *in vitro* selection with the Systematic Evolution of Ligands by EXponential enrichment (SELEX) method. Also, this method is further applied to cells to find cell-specific aptamers using the cell-SELEX method. Compared with other affinity tags, aptamers have many advantages, including small size, non-toxicity, relatively easy preparation and functionalization with no batch-to-batch variations and easy surface immobilization via their functional groups [51–55]. Thus, they can be easily functionalized simultaneously with (-SH) sulfhydryl groups and fluorescent dyes (fluorophores) to be tethered on the surface of AuNRs for both targeting and imaging purposes.

4. Cancer cell sensing with affinity tag-conjugated gold nanorods

Affinity tag-conjugated AuNRs make use of fluorescence, light scattering and PAI techniques in order to sense cancer cells. AuNRs are particularly preferred in these methods for follow-up in hyperthermia therapy of cancer cells. Representative studies are reviewed below.

4.1. Fluorescence imaging of cancer cells

Molecular recognition on specific cell surfaces plays a key role for diagnosis and therapy of cancer cells. The affinity tags responsible for molecular recognition in cancer cells, such as aptamers and antibodies, can sometimes have weak binding strengths towards their molecular target, also known as a biomarker, on cancer cells. This can diminish the signalling and binding affinity towards those targets. Therefore, instead of using single aptamers for molecular recognition, multiple aptamers can be conjugated on a scaffold nanoparticle to generate a multivalent binding platform, which can enhance the signalling and increase the possibility of binding. AuNRs are good scaffold candidates for

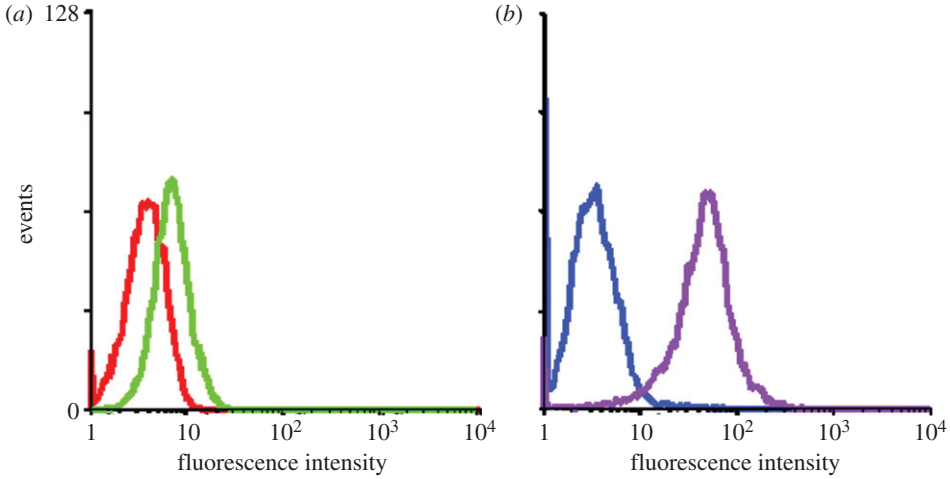

Figure 2. Binding assay of KK1HO8 (50 nM) and NRKK1HO8 conjugates (1.88 nM) towards K-562 cells. (*a*,*b*) The red and blue curves in the flow cytometric assay represent the background binding of unselected DNA library (lib) and NR-conjugated library (NR-lib), respectively. There was an increase in binding capacity of the NRKK1HO8 conjugates (purple curve), whereas there was only a slight change for free KK1HO8 (green curve) with K-562 cells. (Adapted from Huang *et al*. [50]). Copyright © 2008 American Chemical Society.

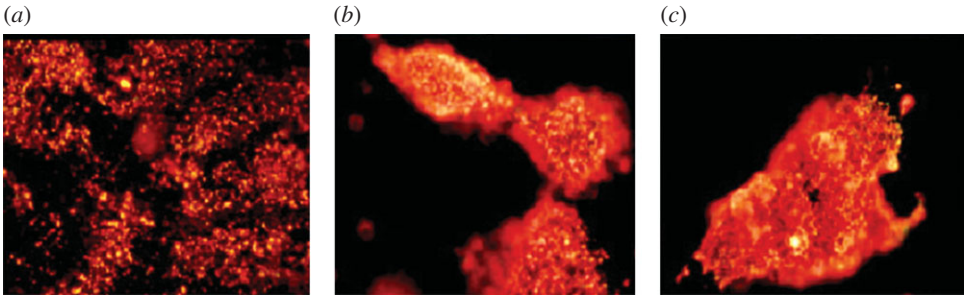

Figure 3. Light scattering images of anti-EGFR/Au nanorods after incubation with cells ((*a*) HaCat non-malignant cells, (*b*) HSC malignant cells and (*c*) HOC malignant cells) for 30 min at room temperature. (Reproduced with permission from Huang *et al*. [24]). Copyright © 2006 American Chemical Society.

multiple aptamers to conjugate, because they can be used as photothermal therapeutic agents following the detection of cancer cells. Huang *et al*. [50] showed that by using the fluorescein-labelled multiple aptamers conjugated to AuNRs, the fluorescence intensity coming from the cell surface is enhanced more than 300-fold compared with those obtained from individual aptamers according to flow cytometric measurements. In this fluorescence signal amplification experiment, the KK1HO8 aptamer that has a weak binding affinity ($K_d \sim 296 \pm 41$ nM) towards K-562 cancer cells was chosen (figure 2). Thus, multiple aptamer-conjugated AuNRs can be a remedy for cases of cancer cells having low expression levels of biomarkers on the cell membrane as binding sites or having aptamers with weak binding affinities towards their binding sites on the cell membrane.

4.2. Light scattering imaging of cancer cells

As was discussed in §2.2, AuNRs can also be used as scattering contrast agents in dark-field imaging. Huang *et al*. used anti-epidermal growth factor receptor (anti-EGFR) monoclonal antibodies conjugated AuNRs to target two malignant oral epithelial cell lines (HSC and HOC) and a non-malignant epithelial cell line (HaCat) was chosen as a control [24]. Because EGFR is over-expressed on the cytoplasmic membrane of malignant cells, the antibody-conjugated AuNRs can bind to the malignant cell lines in a higher affinity compared with the non-malignant cell line. After incubation with each cell line for 30 min at room temperature, the excess AuNRs are washed off. AuNRs that bind to malignant cell lines strongly scatter orange to red light detected by dark-field microcsopy owing to their strong longitudinal surface plasmon oscillation in the NIR region (figure 3). This type of strong scattering can easily be distinguished from the non-malignant cell line. Because the non-malignant cell line also shows scattering as a background, in order to quantify the bound AuNRs on each cell type, absorption spectra of the cell samples incubated with antibody-conjugated AuNRs are taken, and the longitudinal band intensities of AuNRs are compared. The absorption intensities for the malignant cell line samples are two times higher than that for the non-malignant cell line. However, this is not a fair comparison of EGFR expression levels for malignant and non-malignant cell lines, because some of the AuNRs bind to non-malignant cell lines via non-specific interactions, possibly caused by hydrophobic interactions between the PSS on the AuNRs surface (see §3.2) and cell membrane. In spite of this non-specific binding, the cancer cell lines can still easily be distinguished from the non-cancerous cells by the highly efficient scattering properties of AuNRs in the NIR region.

4.3. Photoacoustic imaging of cancer cells

The basic principle of PAI is detection of the sonic waves generated by thermo-elastic expansion of the heated tissue by laser treatment (figure 4; [56]). The sonic waves are

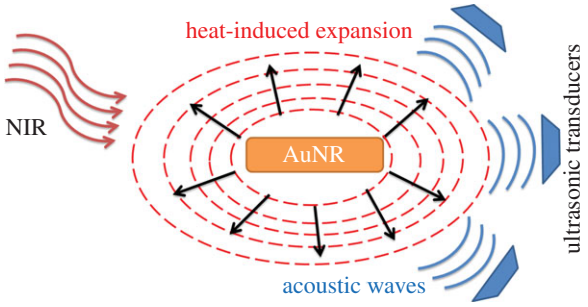

Figure 4. Photoacoustic imaging mechanism.

detected by ultrasonic transducers and converted to electrical signals, followed by processing those electrical signals to form an image.

PAI makes use of the high optical contrast of biological tissues. For example, because of the high optical absorption of haemoglobin (Hb), PAI can image blood vessels successfully [37]. Some *in vivo* studies showed that the ratio between the optical absorption contrasts of normal and tumour tissues in the breast can be as high as 1 : 3 in the NIR region owing to the greatly increased vascularity in the tumours [57–59]. Thus, in contrast to light scattering imaging, PAI requires the contrast agents to have high optical absorption. Owing to their large absorption cross sections in the NIR region (§§2.2 and 2.3), AuNRs are good contrast agent candidates for PAI. The principal of PAI is very similar to the one for photothermal therapy, because heating of the target is involved in both, so it is highly possible to combine these two modalities [37].

Because nanoparticle-based, targeted PAI of cancer is still rather a new technique, there are not so many examples to represent its potential, especially where aptamers are used as affinity tags. The *in vivo* PAI of human prostate cancer is achieved by antibody-conjugated AuNRs [32]. In this study, antibody-conjugated AuNRs are designed to have an absorption band in the range of 700–840 nm to be optimal *in vivo* applications and a single layer of cells is monitored by PAI. In another *in vivo* study, AuNRs in different aspect ratios are conjugated to antibodies to specifically target human epidermal growth factor receptor 2 (HER2) and EGFR, which are over-expressed in OECMI and Cal 27 oral cancer cell lines, respectively. The aspect ratios of the AuNRs that are conjugated to HER2 or EGFR antibodies are tuned to have SPR bands of 785 and 1000 nm, respectively. These two probes are used to target HER2 or EGFR on both oral cancer cell lines, *in vivo* and *in vitro*, while switching the irradiation wavelength to either 800 or 1064 nm for PAI. By matching the irradiation wavelength with the SPR bands of the probes, the corresponding molecular targets for the oral cancer cell lines are successfully monitored by PAI. Even though both probes were not used in the same mice to detect the molecular signatures for the two different cells, by only switching the irradiation wavelength, this work can open new avenues for multiple biomarker detection on cancer cells or for determining heterogeneous population of cancer cells in a lesion [60].

5. Cancer cell therapy with aptamer-conjugated gold nanorods

There are two main methods for administering cancer cell therapy via plasmonic nanoparticles. The first one being photothermal therapy via the heat generation induced by relaxation of the excited surface plasmon electrons, and the second one being the heat-induced drug delivery to cancer cells.

5.1. Photothermal therapy of cancer cells

Cells are highly sensitive to temperature variations, and temperatures above 42°C can result in cell death. Hyperthermia is an anti-cancer therapy that aims to increase the temperature of the cancer cells above normal levels to cause cell death. Excessive heating can induce the denaturation of proteins or the disruption of organized biomolecular assemblies in the nucleus and cytoskeleton of the cells.

In photothermal therapy, NIR lasers are involved for deep tissue penetration and thermal treatment of tumours. This type of therapy requires specificity against cancer cells, in order not to destroy the healthy cells and it also requires sufficient heat generation to kill the targeted cancer cell. Aptamer-conjugated AuNRs can satisfy both of these requirements with specificity provided by the aptamers and efficient heat generation provided by the AuNRs.

Huang *et al*. [26] from the Tan laboratory used aptamer-conjugated AuNRs for selective photothermal therapy in a suspension cell mixture (figure 5). In this study, two cancer cell lines were chosen for the cell mixture: the CCRF-CEM cell line was chosen as a target and the NB-4 cell line was used as a control. The chosen sgc8c aptamer can bind to the membrane protein of the CCRF-CEM cell line, but it cannot bind to any molecular signature on the NB-4 cell line. Also, random DNA library is chosen to serve as a control, indicating the specificity against CCRF-CEM is only because of the sgc8c aptamer. After the sgc8c aptamer and random DNA library are immobilized on the surface of AuNRs (see §3.2), the two cell lines are incubated with the AuNR conjugates separately. After washing off the unbound AuNR conjugates from the cell solutions, the samples are exposed to a laser light of 808 nm at 600 mW for 5 min. Cell death is determined by PI dye staining and monitored by flow cytometry. While CEM cells labelled with sgc8c aptamer-conjugated AuNRs show a cell death percentage of 93 ($\pm$11), the percentage of dead cells before and after laser irradiation remains the same for the NB-4 cell line (figure 6). Also, the percentage of dead cells before and after illumination for the CEM cells incubated with random DNA-library-conjugated AuNRs remains almost the same (2% change). These show the high selectivity of aptamer-conjugated AuNRs against their target cells. Eventually, aptamer-conjugated AuNRs are incubated with a suspension cell mixture of NB-4 and CCRF-CEM cell lines. After NIR laser irradiation, 50 ($\pm$1)% of target (CEM) cells are damaged, whereas 87 ($\pm$1)% of control (NB-4) cells remain intact. These are promising results for future *in vivo* photothermal therapeutic applications, because it is demonstrated that aptamer-conjugated AuNRs are highly selective against the targeted cancer cells and are able to efficiently destroy the targeted cancer cells with minimal damage to the surrounding cells.

5.2. Heat-induced drug delivery to cancer cells

Even though AuNPs can be efficient photothermal agents by tuning their size and shape, their non-porous nanostructures exhibit low loading capacities for effective drug or gene delivery to cancer cells. In order to solve this, Kang *et al*. [35]

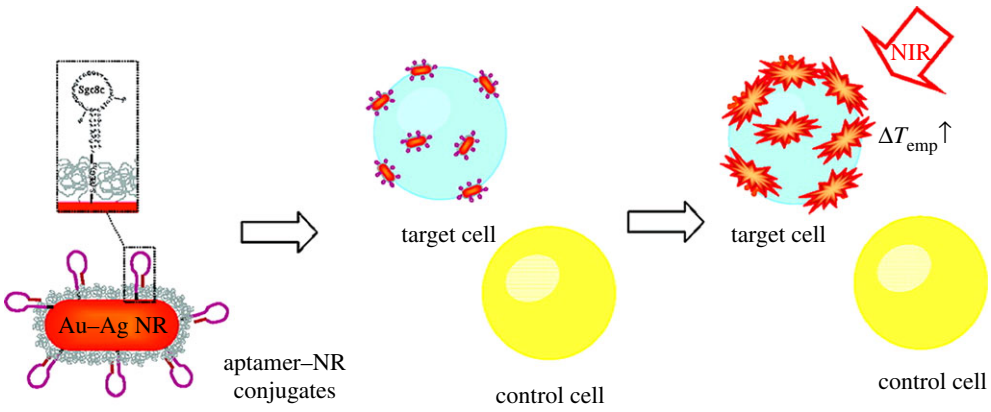

Figure 5. Selective photothermal therapy of cancer cells by aptamer-conjugated AuNRs. (Adapted from Huang *et al*). [26]). Copyright © 2008 American Chemical Society.

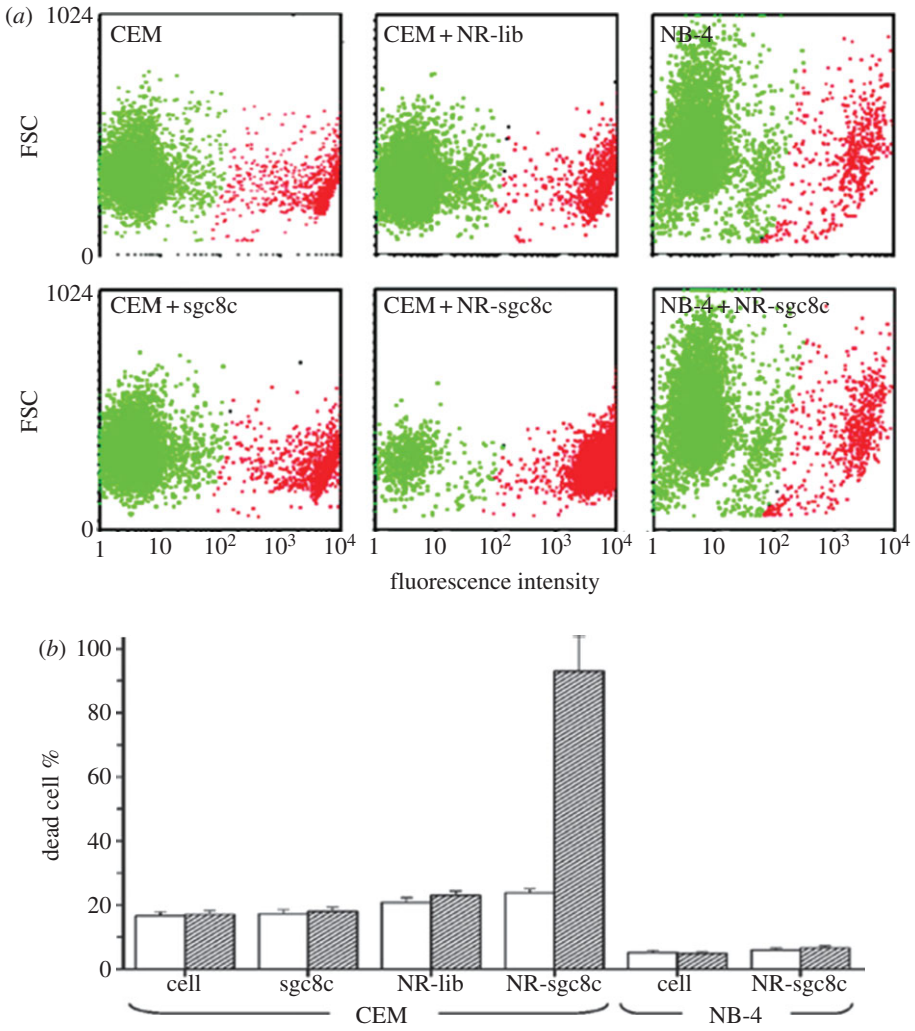

Figure 6. (*a*) Flow cytometric comparison between live and dead cell populations of CCRF-CEM cells (target cells) and NB-4 cells (control cells) without NRs and those labelled with sgc8c (50 nM), NR-lib (0.25 nM) and NR-sgc8c (0.25 nM). A total of 10 µl of the cell suspensions is irradiated with NIR light (808 nm) at 600 mW for 5 min. Dead cells are then stained with PI dye, diluted in buffer and determined by flow cytometry. (*b*) Bar chart demonstrating the dead cell percentages of CCRF-CEM cells (target cells) and NB-4 cells (control cells) in all experimental conditions before (white bar) and after (filled bar) NIR irradiation. (Adapted from Huang *et al*). [26]). Copyright © 2008 American Chemical Society.

engineered a drug delivery platform based on AuNRs coated with DNA cross-linked polymeric shells (figure 7). In this design, acrydite-modified DNA (strand 1) is polymerized on the AuNR surface through copolymerization reactions. Also, another acrydite-modified DNA (strand 2) is polymerized together with acrydite-modified sgc8c aptamer (§5.1) separately. These two polymerized structures are then linked to each other by a linker DNA that is partially complimentary to strand 1 and strand 2 to form a polymeric shell on AuNR. During this AuNR-based nanogel formation, an anticancer drug, Dox, is introduced to be encapsulated in the gel. The basic principle of drug release in this system is the gel-to-sol transition of the gel layer on the AuNR surface caused by the elevated temperatures upon the NIR irradiation,

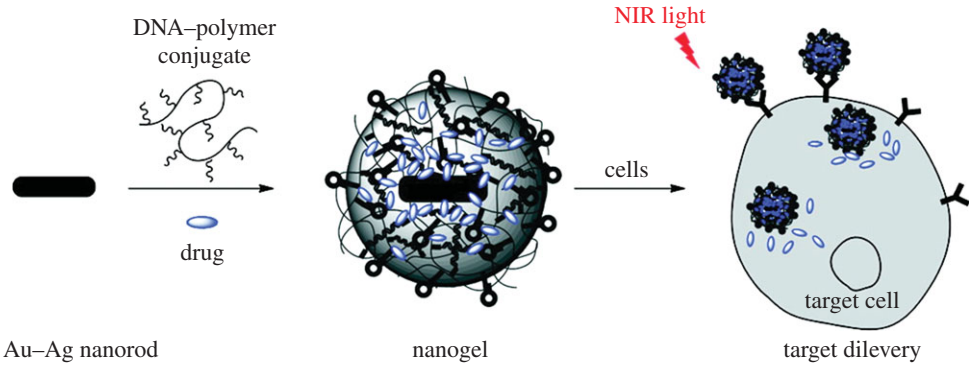

Figure 7. NIR responsive drug delivery platform based on AuNRs coated with DNA cross-linked polymeric shells. (Adapted from Kang *et al*. [35]). Copyright © 2011 American Chemical Society.

in which the encapsulated Dox can be released. This transition depends on the melting temperatures of the linker DNA and the two complementary DNA segments (strand 1 and strand 2). In this case the melting temperature is in the range 35–41°C, but it can be easily tuned by changing the number of hybridized base pairs in the linkage. According to flow cytometry tests, even though acrydite-modified sgc8c aptamers undergo a polymerization reaction, they can still specifically bind to their target cells (CCRF-CEM).

Finally, the drug release of this system is tested by incubation of the target (CCRF-CEM) and control (RAMOS) cells with the Dox-loaded AuNR-based nanogel-sgc8c, followed by exposure to the laser (808 nm at 600 mW). Increasing the irradiation time up to 10 min results in a cell death percentage of 67(±5%) for CEM cells, while the percentage of dead cells remained almost the same (less than 10% change) for RAMOS cells. Also, the same experiment is done with the AuNR-based nanogel-sgc8c without any Dox loading, but the cell death percentage remains almost the same (less than 8% change) for CEM cells. This can indicate that there is minimal contribution from photothermal effect of AuNRs, but cell damage is mainly due to the drug delivery. This study can be inspiring for *in vivo* applications, where the targeted and controlled drug delivery is a big challenge owing to the side effects of the drugs. This system shows that combining the unique features of aptamers and nanoparticles may be a solution for the challenges encountered in real biological applications.

6. Conclusion

Simple changes to the size and shape of AuNPs can give rise to a variety of biomedical applications, because those changes also affect their optical/electronic properties. As reviewed in this paper, by tuning the aspect ratio of AuNRs, their optoelectronic properties can be changed to apply for the desired cancer treatment. However, intrinsic properties of AuNPs are not sufficient to solve the challenges encountered in cancer cell treatments, because without targeting the specific cancer cells, these unique properties will be left on the bench top. Thus, aptamers as targeting tags have an important role in cancer treatments. Currently, not all cancer types have their own aptamers, but in time more aptamers will definitely be selected, which can increase the diversity of cancer treatments.

We would like to thank the American Chemical Society for permission to use adapted figures and Houda Dardari for editing. The reviewed works were supported by State of Florida Center for NanoBiosensors and with the grants from NIH, NCI and NIGMS.

References

1. Connor EE, Mwamuka J, Gole A, Murphy CJ, Wyatt MD. 2005 Gold nanoparticles are taken up by human cells but do not cause acute cytotoxicity. *Small* **1**, 325–327. (doi:10.1002/smll.200400093)
2. Jain PK, Lee KS, El-Sayed IH, El-Sayed MA. 2006 Calculated absorption and scattering properties of gold nanoparticles of different size, shape, and composition: applications in biological imaging and biomedicine. *J. Phys. Chem. B* **110**, 7238–7248. (doi:10.1021/jp057170o)
3. Lee KS, El-Sayed MA. 2006 Gold and silver nanoparticles in sensing and imaging: sensitivity of plasmon response to size, shape, and metal composition. *J. Phys. Chem. B* **110**, 19 220–19 225. (doi:10.1021/jp062536y)
4. Sperling RA, Rivera Gil P, Zhang F, Zanella M, Parak WJ. 2008 Biological applications of gold nanoparticles. *Chem. Soc. Rev.* **37**, 1896–1908. (doi:10.1039/b712170a)
5. Frens G. 1973 Controlled nucleation for the regulation of the particle size in monodisperse gold suspensions. *Nature* **241**, 20–22. (doi:10.1038/physci241020a0)
6. Jana NR, Gearheart L, Murphy CJ. 2001 Seed-mediated growth approach for shape-controlled synthesis of spheroidal and rod-like gold nanoparticles using a surfactant template. *Adv. Mater.* **13**, 1389–1393. (doi:10.1002/1521-4095(200109)13:18<1389::Aid-Adma1389>3.0.Co;2-F)
7. Martin BR, Dermody DJ, Reiss BD, Fang MM, Lyon LA, Natan MJ, Malluok TE. 1999 Orthogonal self-assembly on colloidal gold-platinum nanorods. *Adv. Mater.* **11**, 1021–1025. (doi:10.1002/(Sici)1521-4095(199908)11:12<1021::Aid-Adma1021>3.0.Co;2-S)
8. van der Zande BMI, Böhmer MR, Fokkink LGJ, Schönenberger C. 2000 Colloidal dispersions of gold rods: synthesis and optical properties. *Langmuir* **16**, 451–458. (doi:10.1021/la9900425)
9. Cepak VM, Martin CR. 1998 Preparation and stability of template-synthesized metal nanorod sols in organic solvents. *J. Phys. Chem. B* **102**, 9985–9990. (doi:10.1021/Jp982882i)
10. Govindaraj A, Satishkumar BC, Nath M, Rao CNR. 2000 Metal nanowires and intercalated metal layers in single-walled carbon nanotube bundles. *Chem. Mater.* **12**, 202–205. (doi:10.1021/cm990546o)
11. Jana NR, Gearheart L, Murphy CJ. 2001 Wet chemical synthesis of high aspect ratio cylindrical

gold nanorods. *J. Phys. Chem. B* **105**, 4065–4067. (doi:10.1021/Jp0107964)

12. Nikoobakht B, El-Sayed MA. 2003 Preparation and growth mechanism of gold nanorods (NRs) using seed-mediated growth method. *Chem. Mater.* **15**, 1957–1962. (doi:10.1021/Cm020732l)
13. Grzelczak M, Perez-Juste J, Mulvaney P, Liz-Marzan LM. 2008 Shape control in gold nanoparticle synthesis. *Chem. Soc. Rev.* **37**, 1783–1791. (doi:10.1039/b711490g)
14. Ahmadi TS, Wang ZL, Green TC, Henglein A, El-Sayed MA. 1996 Shape-controlled synthesis of colloidal platinum nanoparticles. *Science* **272**, 1924–1926. (doi:10.1126/science.272.5270.1924)
15. Huang CC, Huang YF, Cao Z, Tan W, Chang HT. 2005 Aptamer-modified gold nanoparticles for colorimetric determination of platelet-derived growth factors and their receptors. *Anal. Chem.* **77**, 5735–5741. (doi:10.1021/ac050957q)
16. Lin TE, Chen WH, Shiang YC, Huang CC, Chang HT. 2011 Colorimetric detection of platelet-derived growth factors through competitive interactions between proteins and functional gold nanoparticles. *Biosens. Bioelectron.* **29**, 204–209. (doi:10.1016/j.bios.2011.08.020)
17. Chen CK, Huang CC, Chang HT. 2010 Label-free colorimetric detection of picomolar thrombin in blood plasma using a gold nanoparticle-based assay. *Biosens. Bioelectron.* **25**, 1922–1927. (doi:10.1016/j.bios.2010.01.005)
18. Xia F *et al*. 2010 Colorimetric detection of DNA, small molecules, proteins, and ions using unmodified gold nanoparticles and conjugated polyelectrolytes. *Proc. Natl Acad. Sci. USA* **107**, 10 837–10 841. (doi:10.1073/pnas.1005632107)
19. Elghanian R, Storhoff JJ, Mucic RC, Letsinger RL, Mirkin CA. 1997 Selective colorimetric detection of polynucleotides based on the distance-dependent optical properties of gold nanoparticles. *Science* **277**, 1078–1081. (doi:10.1126/science.277.5329.1078)
20. Storhoff JJ, Elghanian R, Mucic RC, Mirkin CA, Letsinger RL. 1998 One-pot colorimetric differentiation of polynucleotides with single base imperfections using gold nanoparticle probes. *J. Am. Chem. Soc.* **120**, 1959–1964. (doi:10.1021/ja972332i)
21. Storhoff JJ, Lazarides AA, Mucic RC, Mirkin CA, Letsinger RL, Schatz GC. 2000 What controls the optical properties of DNA-linked gold nanoparticle assemblies? *J. Am. Chem. Soc.* **122**, 4640–4650. (doi:10.1021/ja993825l)
22. Medley CD, Smith JE, Tang Z, Wu Y, Bamrungsap S, Tan W. 2008 Gold nanoparticle-based colorimetric assay for the direct detection of cancerous cells. *Anal. Chem.* **80**, 1067–1072. (doi:10.1021/ac702037y)
23. Hirsch LR, Stafford RJ, Bankson JA, Sershen SR, Rivera B, Price RE, Hazle JD, Halas NJ, West JL. 2003 Nanoshell-mediated near-infrared thermal therapy of tumors under magnetic resonance guidance. *Proc. Natl Acad. Sci. USA* **100**, 13 549–13 554. (doi:10.1073/pnas.2232479100)
24. Huang X, El-Sayed IH, Qian W, El-Sayed MA. 2006 Cancer cell imaging and photothermal therapy in the near-infrared region by using gold nanorods. *J. Am. Chem. Soc.* **128**, 2115–2120. (doi:10.1021/ja057254a)
25. Dickerson EB, Dreaden EC, Huang X, El-Sayed IH, Chu H, Pushpanketh S, Mcdonald J, Elsayed M. 2008 Gold nanorod assisted near-infrared plasmonic photothermal therapy (PPTT) of squamous cell carcinoma in mice. *Cancer Lett.* **269**, 57–66. (doi:10.1016/j.canlet.2008.04.026)
26. Huang YF, Sefah K, Bamrungsap S, Chang HT, Tan W. 2008 Selective photothermal therapy for mixed cancer cells using aptamer-conjugated nanorods. *Langmuir* **24**, 11 860–11 865. (doi:10.1021/la801969c)
27. Goodrich GP, Bao L, Gill-Sharp K, Sang KL, Wang J, Payne JD. 2010 Photothermal therapy in a murine colon cancer model using near-infrared absorbing gold nanorods. *J. Biomed. Opt.* **15**, 018001. (doi:10.1117/1.3290817)
28. Chen J *et al*. 2007 Immuno gold nanocages with tailored optical properties for targeted photothermal destruction of cancer cells. *Nano Lett.* **7**, 1318–1322. (doi:10.1021/nl070345g)
29. Wang YW, Xie XY, Wang XD, Ku G, Gill KL, O'Neal DP, Stoica G, Wang LV. 2004 Photoacoustic tomography of a nanoshell contrast agent in the *in vivo* rat brain. *Nano Lett.* **4**, 1689–1692. (doi:10.1021/Nl049126a)
30. Eghtedari M, Oraevsky A, Copland JA, Kotov NA, Conjusteau A, Motamedi M. 2007 High sensitivity of *in vivo* detection of gold nanorods using a laser optoacoustic imaging system. *Nano Lett.* **7**, 1914–1918. (doi:10.1021/nl070557d)
31. Li P-C, Wei C-W, Liao CK, Chen CD, Pao KC, Wang C-RC, Wu Y-N, Shieh DB. 2006 Multiple targeting in photoacoustic imaging using bioconjugated gold nanorod. *Proc. SPIE* **6086**, 60860M. (doi:10.1117/12.645248)
32. Agarwal A, Huang SW, O'Donnell M, Day KC, Day M, Kotov N, Ashkenazi S. 2007 Targeted gold nanorod contrast agent for prostate cancer detection by photoacoustic imaging. *J. Appl. Phys.* **102**, 064701. (doi:10.1063/1.2777127)
33. Song KH, Kim C, Maslov K, Wang LV. 2009 Noninvasive *in vivo* spectroscopic nanorod-contrast photoacoustic mapping of sentinel lymph nodes. *Eur. J. Radiol.* **70**, 227–231. (doi:10.1016/j.ejrad.2009.01.045)
34. Yang X, Skrabalak SE, Li ZY, Xia Y, Wang LV. 2007 Photoacoustic tomography of a rat cerebral cortex *in vivo* with Au nanocages as an optical contrast agent. *Nano Lett.* **7**, 3798–3802. (doi:10.1021/nl072349r)
35. Kang H *et al.* 2011 Near-infrared light-responsive core-shell nanogels for targeted drug delivery. *ACS Nano* **5**, 5094–5099. (doi:10.1021/nn201171r)
36. Anderson RR, Parrish JA. 1981 The Optics of Human-Skin. *J. Invest. Dermatol.* **77**, 13–19. (doi:10.1111/1523-1747.Ep12479191)
37. Yang X, Stein EW, Ashkenazi S, Wang LV. 2009 Nanoparticles for photoacoustic imaging. *Wiley Interdiscip. Rev. Nanomed. Nanobiotechnol.* **1**, 360–368. (doi:10.1002/wnan.42)
38. Huang X, El-Sayed I, El-Sayed M. 2010 Applications of gold nanorods for cancer imaging and photothermal therapy. In *Cancer nanotechnology* (eds SR Grobmyer, BM Moudgil), pp. 343–357. New York, NY: Humana Press.
39. Didychuk CL, Ephrat P, Chamson-Reig A, Jacques SL, Carson JJL. 2009 Depth of photothermal conversion of gold nanorods embedded in a tissue-like phantom. *Nanotechnology* **20**, 195102. (doi:10.1088/0957-4484/20/19/195102)
40. Kennedy LC, Bickford LR, Lewinski NA, Coughlin AJ, Hu Y, Day ES, West JL, Drezek RA. 2011 A new era for cancer treatment: gold-nanoparticle-mediated thermal therapies. *Small* **7**, 169–183. (doi:10.1002/smll.201000134)
41. Hu M, Chen JY, Li ZY, Au L, Hartland GV, Li XD, Marquez M, Xia Y. 2006 Gold nanostructures: engineering their plasmonic properties for biomedical applications. *Chem. Soc. Rev.* **35**, 1084–1094. (doi:10.1039/B517615h)
42. Lee KS, El-Sayed MA. 2005 Dependence of the enhanced optical scattering efficiency relative to that of absorption for gold metal nanorods on aspect ratio, size, end-cap shape, and medium refractive index. *J. Phys. Chem. B* **109**, 20 331–20 338. (doi:10.1021/jp054385p)
43. von Maltzahn G, Park JH, Agrawal A, Bandaru NK, Das SK, Sailor MJ, Bhatia SN. 2009 Computationally guided photothermal tumor therapy using long-circulating gold nanorod antennas. *Cancer Res.* **69**, 3892–3900. (doi:10.1158/0008-5472.CAN-08-4242)
44. Esumi K, Matsuhisa K, Torigoe K. 1995 Preparation of rodlike gold particles by UV irradiation using cationic micelles as a template. *Langmuir* **11**, 3285–3287. (doi:10.1021/La00009a002)
45. Yu Y, Chang S-S, Lee C-L, Wang CRC. 1997 Gold nanorods: electrochemical synthesis and optical properties. *J. Phys. Chem. B* **101**, 6661–6664. (doi:10.1021/jp971656q)
46. Murphy CJ, Sau TK, Gole AM, Orendorff CJ, Gao J, Gou L, Hunyadi SE, Li T. 2005 Anisotropic metal nanoparticles: synthesis, assembly, and optical applications. *J. Phys. Chem. B* **109**, 13 857–13 870. (doi:10.1021/jp0516846)
47. Perezjuste J, Pastorizasantos I, Lizmarzan L, Mulvaney P. 2005 Gold nanorods: synthesis, characterization and applications. *Coord. Chem. Rev.* **249**, 1870–1901. (doi:10.1016/j.ccr.2005.01.030)
48. Cheng PC, Chang HK, Chen SH. 2010 Quantitative nanoproteomics for protein complexes (QNanoPX) related to estrogen transcriptional action. *Mol. Cell. Proteomics* **9**, 209–224. (doi:10.1074/mcp.M900183-MCP200)
49. Yasun E, Gulbakan B, Ocsoy I, Yuan Q, Shukoor MI, Li C, Tan W. 2012 Enrichment and detection of rare proteins with aptamer-conjugated gold nanorods. *Anal. Chem.* **84**, 6008–6015. (doi:10.1021/ac300806s)
50. Huang YF, Chang HT, Tan W. 2008 Cancer cell targeting using multiple aptamers conjugated on nanorods. *Anal. Chem.* **80**, 567–572. (doi:10.1021/ac702322j)

51. Sefah K, Phillips JA, Xiong X, Meng L, Van Simaeys D, Chen H, Martin J, Tan W. 2009 Nucleic acid aptamers for biosensors and bio-analytical applications. *Analyst* **134**, 1765–1775. (doi:10.1039/b905609m)
52. Meir A, Marks RS, Stojanovic MN. 2008 *Aptameric biosensors. Handbook of biosensors and biochips*. New York, NY: John Wiley & Sons, Ltd.
53. Mallikaratchy P, Tang Z, Kwame S, Meng L, Shangguan D, Tan W. 2007 Aptamer directly evolved from live cells recognizes membrane bound immunoglobin heavy mu chain in Burkitt's lymphoma cells. *Mol. Cell. Proteomics* **6**, 2230–2238. (doi:10.1074/mcp.M700026-MCP200)
54. Shangguan D, Tang Z, Mallikaratchy P, Xiao Z, Tan W. 2007 Optimization and modifications of aptamers selected from live cancer cell lines. *ChemBioChem* **8**, 603–606. (doi:10.1002/cbic.200600532)
55. Shangguan D, Cao Z, Meng L, Mallikaratchy P, Sefah K, Wang H, Li Y, Tan W. 2008 Cell-specific aptamer probes for membrane protein elucidation in cancer cells. *J. Proteome Res.* **7**, 2133–2139. (doi:10.1021/pr700894d)
56. Yuan Z, Jiang H. 2010 Photoacoustic tomography for imaging nanoparticles. In *Cancer nanotechnology* (eds SR Grobmyer, BM Moudgil), pp. 309–324. New York, NY: Humana Press.
57. Jiang H, Iftimia NV, Xu Y, Eggert JA, Fajardo LL, Klove KL. 2002 Near-infrared optical imaging of the breast with model-based reconstruction. *Acad. Radiol.* **9**, 186–194. (doi:10.1016/S1076-6332(03)80169-1)
58. Ntziachristos V, Yodh AG, Schnall M, Chance B. 2000 Concurrent MRI and diffuse optical tomography of breast after indocyanine green enhancement. *Proc. Natl Acad. Sci. USA* **97**, 2767–2772. (doi:10.1073/pnas.040570597)
59. Cerussi AE, Berger AJ, Bevilacqua F, Shah N, Jakubowski D, Butler J, Holcombe RF, Tromberg BJ. 2001 Sources of absorption and scattering contrast for near-infrared optical mammography. *Acad. Radiol.* **8**, 211–218. (doi:10.1016/S1076-6332(03)80529-9)
60. Li PC, Wang CRC, Shieh DB, Wei CW, Liao CK, Poe C, Jhan S, Ding A-A, Wu Y-N. 2008 *In vivo* photoacoustic molecular imaging with simultaneous multiple selective targeting using antibody-conjugated gold nanorods. *Opt. Express* **16**, 18 605–18 615. (doi:10.1364/OE.16.018605)